In-situ Observation of Mixed Mode Fatigue Crack Growth Behavior in Heat Affected Zone of a Welded Joint

Ming-Liang Zhu*, De-Qiang Wang, Fu-Zhen Xuan, Shan-Tung Tu

Key Laboratory of Pressure Systems and Safety, Ministry of Education, East China University of Science and Technology, Shanghai 200237, China
* Corresponding author: mlzhu@ecust.edu.cn

Abstract In-situ scanning electron microscope (SEM) observations of fatigue crack growth behavior in heat affected zone (HAZ) of a welded joint were performed with CTS (Compact-Tension-Shear) specimens under mixed-mode loading conditions in vacuum. Results showed that mode I fatigue behavior in the HAZ was influenced by local microstructure anisotropy and the 'zigzag' mode crack profile tended to deviate into the lower strength weld metal. With increasing the mixity of mode I/II loadings, fatigue crack growth rate was decreased with significant crack branching. Shear and branch cracks were competitive along the crack path, and fatigue cracks were often initiated from grain boundary and the interface of lath martensites. The cracks tended to orient themselves into a pure mode I condition. Three existing models were discussed with respect to their capabilities to predict crack direction under various loading conditions.

Keywords in-situ SEM, fatigue crack growth, crack growth path, mixed-mode loading, heat affected zone

1. Introduction

Generally, the various loading types in actual practices are often idealized as being mode I, mode II and mode III based on linear elastic fracture mechanics. Majority of crack growth investigations under both static and cyclic loadings were concentrated on single-mode loading mode such as the mode-I load condition. Unfortunately, single-mode loading seldom occurs in practice, and many service failures occur from cracks subjected to mixed mode loadings which involve more than one crack-tip mode. Even in pure mode I cyclic testing, any deviation of crack path or alternation of external loading direction would lead to combinations of mode II deformation in crack growth process.

Under mixed mode loading conditions, it was of importance to consider the evolution of crack growth direction. Several criteria for crack growth path prediction such as maximum tangential stress (MTS) criterion by Erdogan and Sih [1], minimum strain energy density (SED) criterion by Sih [2], the criterion of energy release rates by Nuismer [3], and the criterion of Richard [4], have been proposed and well documented in [4-6]. However, all these concepts were based on the isotropic material and limited to the linear elastic fracture mechanics [5]. Another issue in combined loading mode was the crack growth rate. Unlike the conventional stress intensity factor range ΔK in pure mode I fatigue, many parameters have been proposed to correlate mixed mode fatigue crack growth (FCG) rates. For example, Tanaka [7] and Yan [8] suggested the effective stress intensity factor range ΔK_{eff}, Patel and Pandey [9] insisted the strain energy density factor range ΔS, while Socie et al [10] proposed the equivalent strain intensity factor for small cracks.

Moreover, the fatigue thresholds [11, 12], crack closure [13, 14], microstructure [15] and loading path [16, 17] influences under mixed mode loading conditions have been investigated. While cracks were observed to propagate in homogeneous materials as widely reported, complications associated with the mixed mode fatigue crack behavior in heterogeneous microstructures, i.e., the gradient microstructures in the heat-affected-zone (HAZ), were far less well understood. In this case, the effect of microstructure anisotropy on crack growth morphology needed to be elucidated.

In the present work, mixed mode (I+II) FCG experiments were performed on an in-situ stage equipped in SEM by using CTS (Compact-Tension-Shear) specimens developed by Richard [18]. The effect of external loading angle on the crack growth rate and crack growth direction was analyzed in terms of local microstructure gradient in the HAZ. The crack growth direction was finally predicted on the basis of the existing models.

2. Materials and experiments

2.1. Materials and specimens

The material studied was the HAZ of a welded joint. The base material of the welding joint was a NiCrMoV type steel. It was undergone quenching and tempering heat treatment, and the resultant tensile strength and yield strength were 835.5 and 938 MPa, respectively. The weldment was formed by submerged arc welding (SAW) technique using filler metal of the 2.5%Ni low alloy steel. The HAZ, which had a width of about 3 mm, included three micro-zones, i.e., fully quenched-tempered zone (FQTZ), partially quenched-tempered zone (PQTZ) and tempered zone (TZ) [19]. The microstructures mainly included tempered martensites and bainites with martensite/bainite constituents altered in the HAZ.

In order to prepare CTS specimen for in-situ observation, standard three-point bending samples with a/W ratio of 0.5 and the thickness B of 16 mm were firstly machined from the welded joint. The initial notch in the sample was located in the FQTZ of the HAZ, with a distance of 120 μm to the fusion line. The samples were then pre-cracked under pure mode I loading at a stress ratio of 0.1 with a sinusoidal waveform to form a crack length of about 2 mm. Subsequently, relatively smaller specimens with a thickness of about 0.5 mm were prepared for in-situ tests. Fig. 1 shows the shape and dimensions of the CTS specimens.

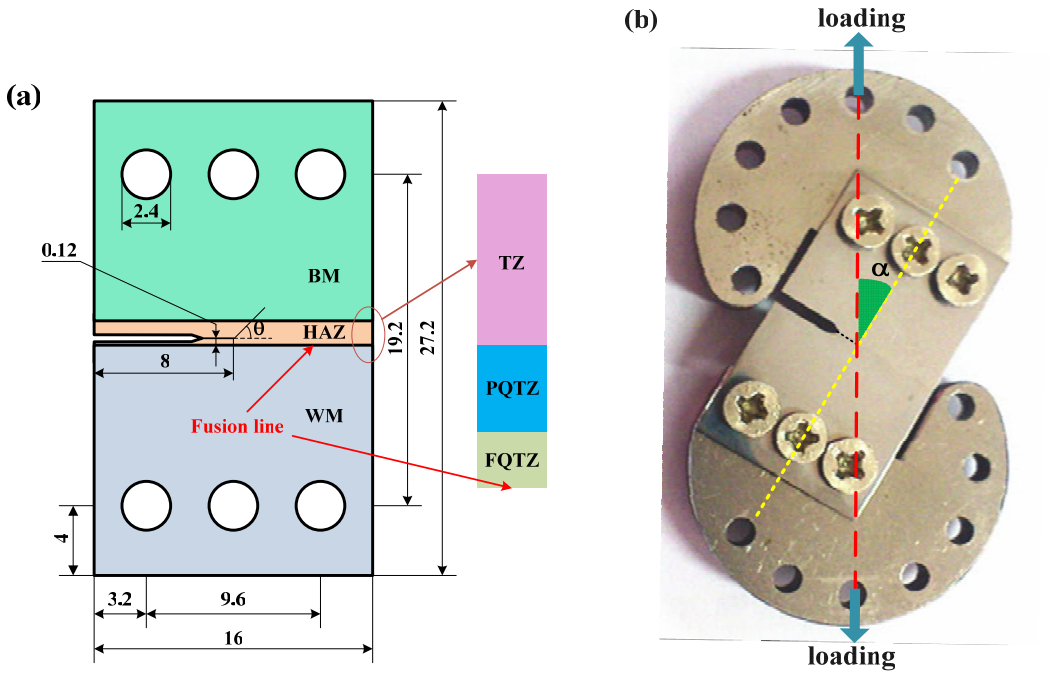

Figure 1. The shape and dimensions of the CTS specimens (a) and the loading device for mixed mode tests (b)

2.2. Fatigue experiments

Before the in-situ fatigue experiments, the CTS specimens were grounded, polished and finally

etched. Constant amplitude fatigue tests using triangular waveform with a load ratio of 0.1were performed on a loading stage equiped in the SEM in vacuum environment (9×10^{-4}–9×10^{-3} Pa). The frequency was as low as 0.03 Hz. The various values of $\Delta K_I/\Delta K_{II}$ could be achieved by changing the external loading angle α. As shown in Fig. 1b, the line of application of force F extends at an angle α to the longitudinal axis of the specimen. Depending on the size of angle α, mixed mode loadings occur at $0<\alpha<90°$. It is obvious that pure mode I loading corresponds to the α equaling to zero, whereas the α at 90° stands for the pure mode II loading. After the crack extended for a given length (less than 10 μm), the experiments were intermitted to measure crack length, record the cyclic numbers and characterize the crack morphology as well. For various loading angles, the initial mixed mode fatigue crack growth parameters, which was calculated by the Eqs. (1) - (3) developed by Richard [17], are listed in Table.1. In Eq. (3), the material parameter α_1 is set to 1.155.

$$K_{\mathrm{I}} = \frac{F\sqrt{\pi a}}{WB}\cdot\frac{\cos\alpha}{1-a/W}\cdot\sqrt{\frac{0.26+2.65\cdot\frac{a}{W-a}}{1+0.55\cdot\frac{a}{W-a}-0.08\cdot\left(\frac{a}{W-a}\right)^2}} \tag{1}$$

$$K_{\mathrm{II}} = \frac{F\sqrt{\pi a}}{WB}\cdot\frac{\sin\alpha}{1-a/W}\cdot\sqrt{\frac{-0.23+1.40\cdot\frac{a}{W-a}}{1-0.67\cdot\frac{a}{W-a}+2.08\cdot\left(\frac{a}{W-a}\right)^2}} \tag{2}$$

$$\Delta K_{\mathrm{eff}} = \frac{K_{\mathrm{I}}}{2}+\frac{1}{2}\sqrt{K_{\mathrm{I}}^2+4\left(\alpha_1 K_{\mathrm{II}}\right)^2} \tag{3}$$

Table 1. Initial mixed mode FCG parameters in the FQTZ of the HAZ

α	a_0/W	ΔK_I (MPa·m$^{1/2}$)	ΔK_{II} (MPa·m$^{1/2}$)	$\Delta K_I/\Delta K_{eff}$
0	0.5451	35.27	0	1
30°	0.5449	30.46	7.95	0.92
60°	0.5476	17.75	13.82	0.65

3. Results

3.1. *a*-*N* relationship

Fig. 2 shows the changes of crack extension as a function of cyclic numbers. It is observed that the crack extends slowly first and then become faster at all of the loading angles. However, with the decreasing of $\Delta K_I/\Delta K_{eff}$, which meant the reduced contribution of mode I loading, the crack extension was also decreased. Nevertheless, due to the proximity of the $\Delta K_I/\Delta K_{eff}$ values at α of zero and 30°, the corresponding crack extension values were also close and even converged to each other eventually. This indicated that the load mixity dependence of crack growth behavior located mainly in the initial crack growth process.

3.2. Fatigue crack growth rate d*a*/d*N*

Fig. 3 indicates the FCG rate da/dN at various loading angles. It is worth noting that the da/dN at α of zero and 30° are similar to each other but larger than those of the α of 60°. It is also worth noting that the evolution of da/dN for pure mode I loading fluctuates with the crack length, i.e., the delay and acceleration phases alternates. This reflected the influence of local microstructures. Whereas for

mixed mode of fatigue, the da/dN are tended to increase along with the crack length at both α of 30° and 60°. In this case, the important issue is that whether the local microstructures still have a large influence or are there other factors that should be considered. The roles of ΔK_{I} and ΔK_{II} in the mixed mode crack growth also need to be elucidated.

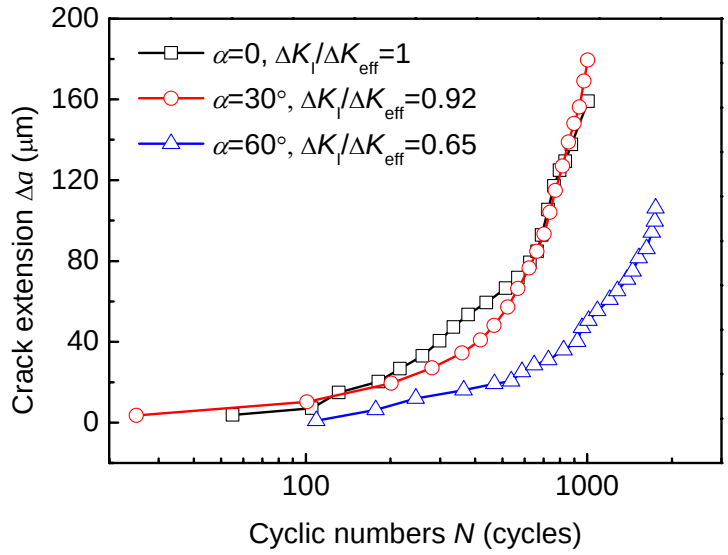

Figure 2. The crack extension Δa versus cyclic numbers N at different loading angles

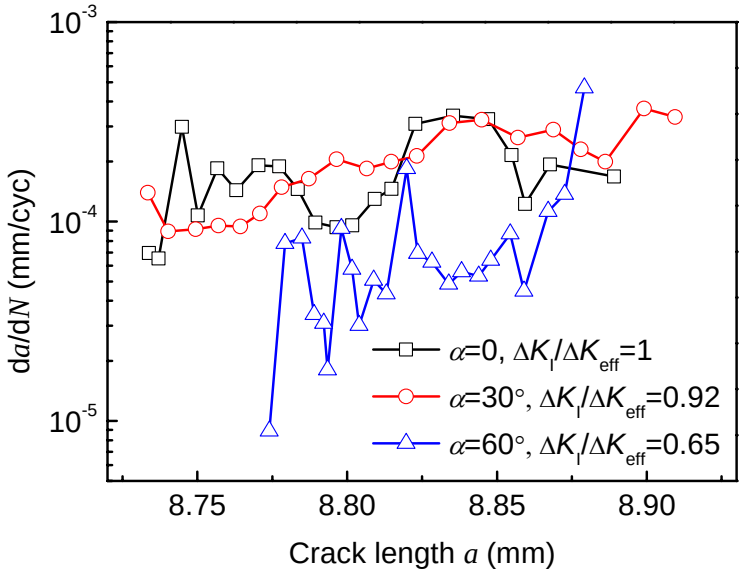

Figure 3. Fatigue crack growth rates at different loading angles

3.3. Crack growth path deflection

Fig. 4 presents the macro-crack profile at various loading angles. For mode I loading, as shown in Fig. 4a, crack deflected for about 21° from the initial pre-crack and then fluctuated, and the resultant crack path was quite tortuous. When load mode was superimposed with mode II loading at α of 30° (Fig. 4b), the initial angles of branch cracks was increased to 27°. Under this angle, crack extended for about 150 μm, after which the crack was further deviated to an angle of about 45° in

the final stage of growth of 40 μm. With the ΔK_{II} further increased, i.e., α equals 60° in Fig. 4c, the initial branch cracks deflected about 52°. The crack extension values along the crack path in the X and Y-axis directions are depicted in Fig. 5. By linear fitting of the data, the deflection angles were consequently calculated to be 25° and 50° at α of 30° and 60°, respectively. This agreed well with the work reported by Kim [20] who obtained similar values in a rail steel.

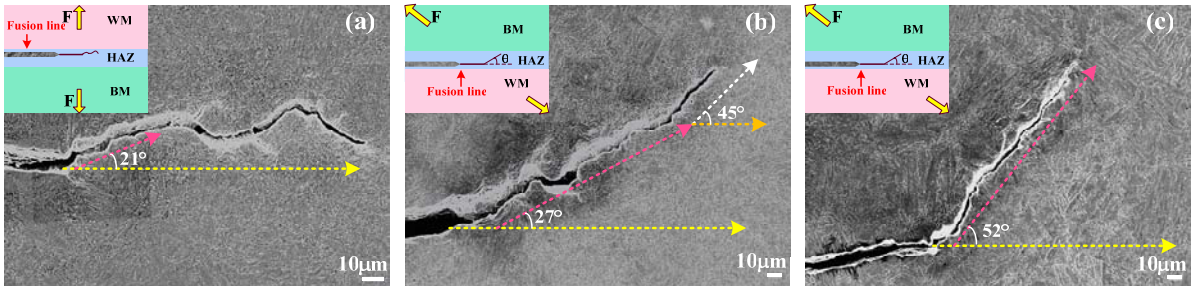

Figure 4. Macro-crack growth path at various loading angles: (a) α = 0, (b) α = 30°, and (c) α = 60°

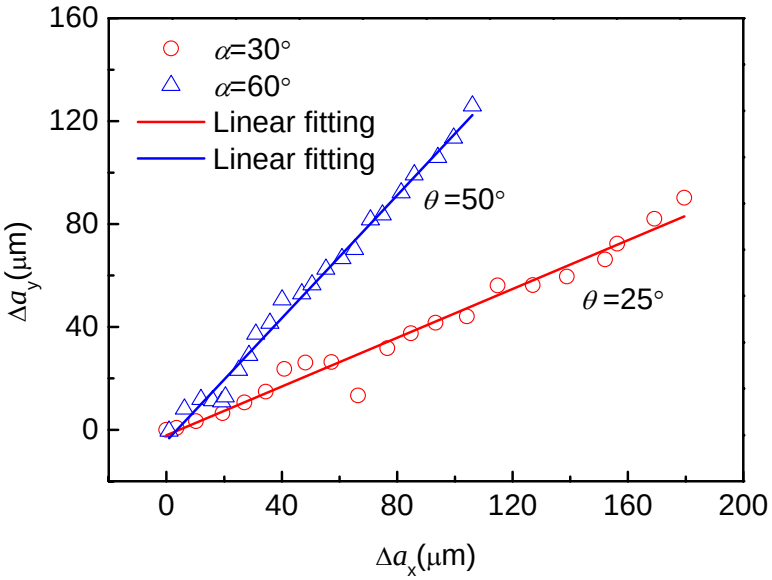

Figure 5. Fatigue crack extension in mixed mode loading conditions

4. Discussion

4.1. Influence of loading angle on FCG

Fig. 6 shows the FCG under pure mode I loading. At the end of the pre-crack, the crack propagated with two branches, as illustrated in Fig. 6b. One of the branch crack (lower side of the pre-crack) stopped growth after initiation along the grain boundary, whereas the other branch crack deflected at an angle of 21° and propagated to become the main crack. The competition between the two branch cracks to form the main crack was observed at *N* around 513 cycles in Fig. 6c. Though the original main crack continued growing forward, the lower side branch crack grew with a higher rate in a transgranular mode, and finally produced the main crack (Fig. 6d). In this process, it seemed that the crack tended to orient itself into a pure mode I condition at which the crack path was normal to the external loading direction.

The alternation of the main crack was also observed when *N* was around 727 cycles, as shown in

Figs. 6e and f. In this case, the main crack was finally formed by propagating the short branch crack and the non-propagation of the original main crack (the lower side branch crack in Fig. 6e). With the crack length increasing, as indicated in Fig. 6g, the slanted crack was again prone to return to the pure mode I trajectory, producing multiple bifurcations along the curved crack path. The bifurcated cracks were often located at grain boundaries and martensite lath interfaces. It is worth noting that the overall crack path propagated with serious local deviations, showing a 'zigzag' mode.

It is inferred that the significant changes of crack orientation is due to the highly anisotropic microstructures at the crack tip and the gradient strength distribution in the HAZ. It is generally accepted that the crack path is governed by the plastic behavior of the crack tip [21]. Accordingly, the cracks would orient themselves into the materials with lower strength values. Therefore, it is reasonable that the crack path is tended to deflect into the weld metal, which has lower strength than the PQTZ in the HAZ.

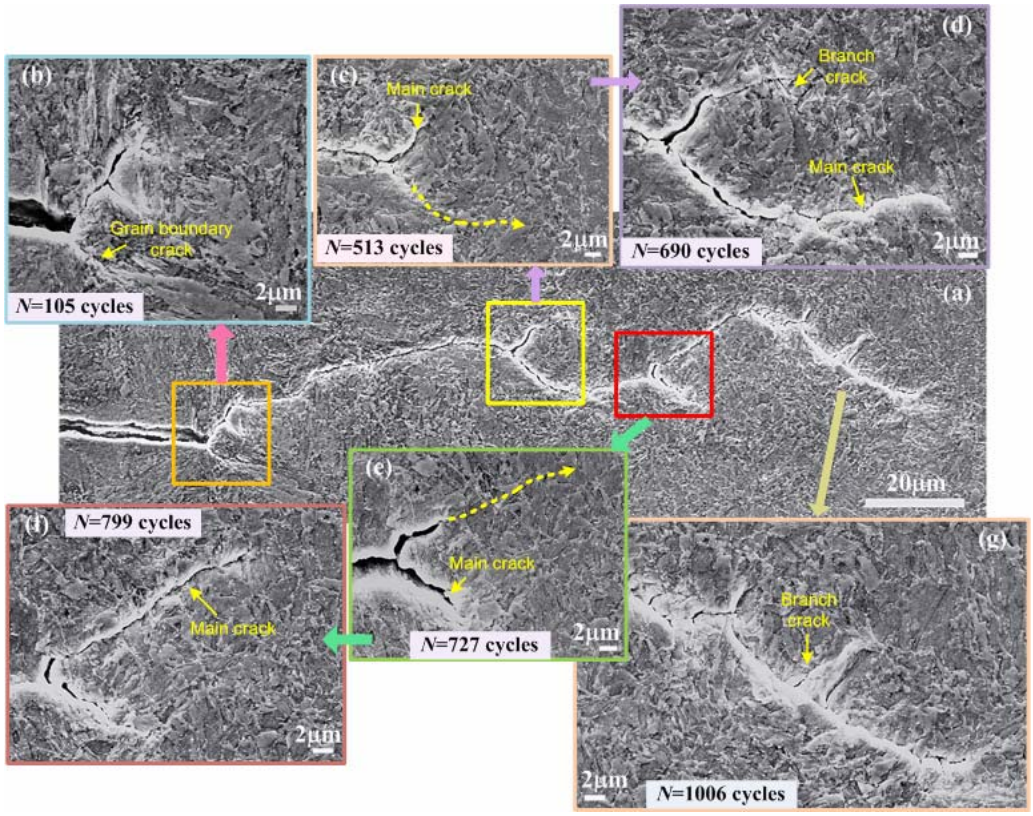

Figure 6. Fatigue crack growth morphology in pure mode I loading

Fig. 7 presents the FCG path at a loading angle of 30°. In Fig. 7a, the crack direction changed immediately from the initial pre-crack orientation with an angle of 27°. Crack bifurcations and shear cracks coexisted along with the main crack, which was resulted from the contribution of mode I and II components. As a result, the mode I component would drive the branch crack for a long length to a mode I crack direction. This was evidenced by formation of main crack based on the original branch crack in Fig. 7b. Tong et al. [22] reported that the formation and propagation of mode I branch cracks were of decisive importance for fatigue failures under combined loadings. It is also observed that the crack tip in Fig. 7a is branched along the grain boundary when N is increased to 622 cycles. On the other hand, the mode II component also contributed to FCG. With the formation of the grain boundary cracks at crack tip in Fig. 7b, a damage area containing many micro-cracks whose direction were almost parallel to the main crack was also formed, as shown in Fig. 7c. This was arisen from the shear deformation under mode II component in the mixed mode

loading.

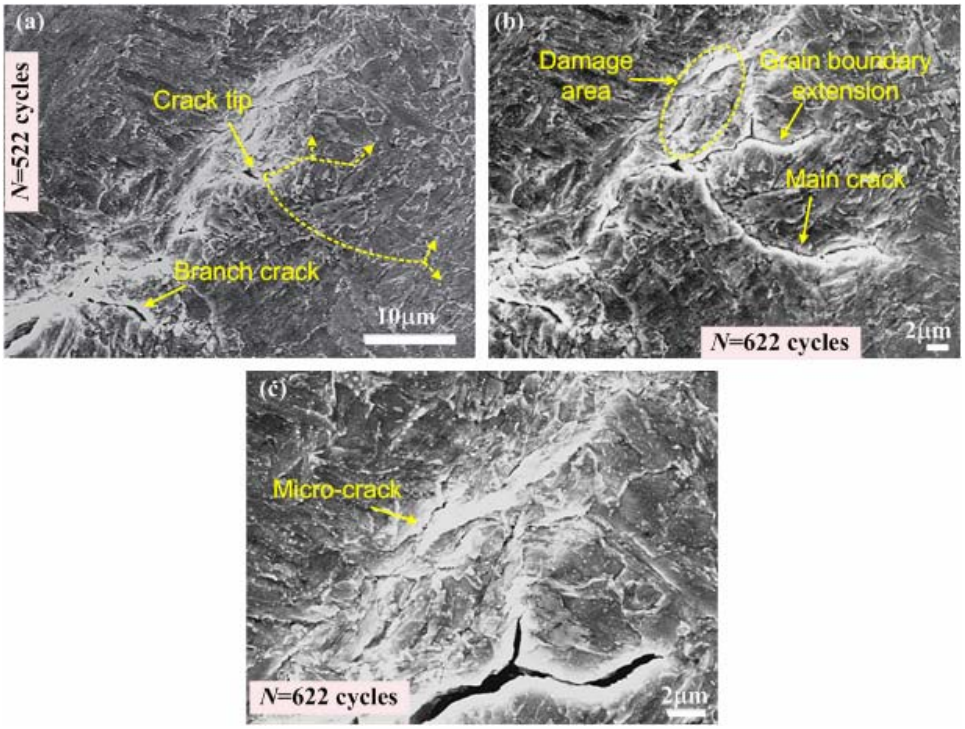

Figure 7. Fatigue crack growth path at a loading angle of 30°

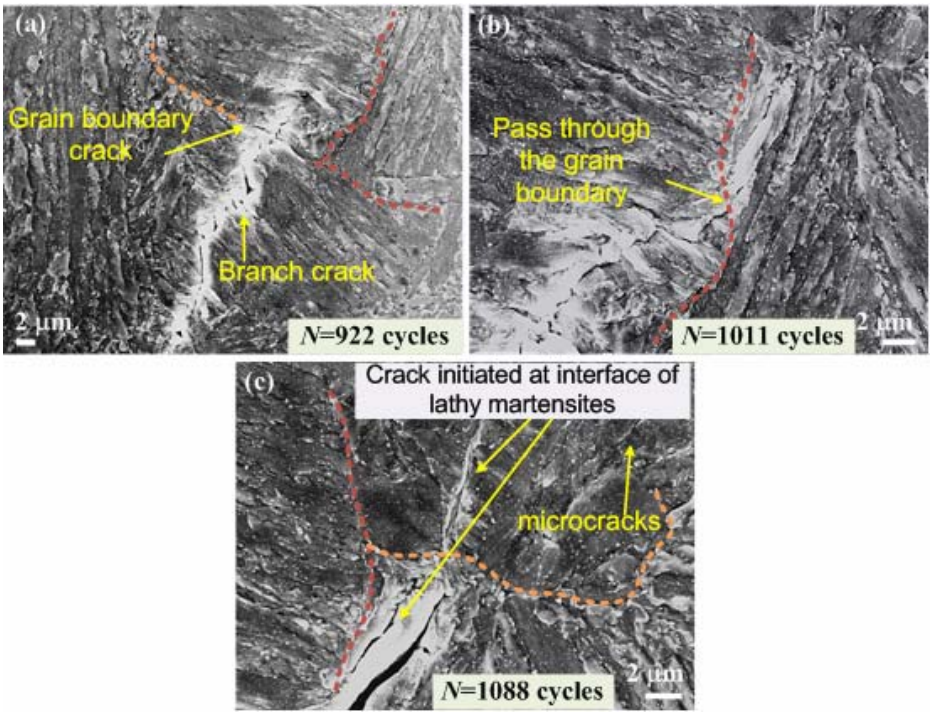

Figure 8. Fatigue crack growth path at a loading angle of 60°

The FCG behavior at a loading angle of 60° is illustrated in Fig. 8. It is observed in Fig. 8a that the crack extends transversely among the lathy martensites and propagates directly through the grain boundaries. In this process, crack bifurcated along the lath interfaces and grain boundaries. The passing through of the crack into the grain boundary was also observed in Fig. 8b, and then the crack extended along the interface of the lathy martensites. Therefore, it can be concluded that the interfaces of lathy martensites and the grain boundary are potential crack initiation sites. With the

increasing of cyclic numbers, one crack was formed again along the interface of the lathy martensites in the nearby grains, as can be seen in Fig. 8c. This would provide an easy path for the crack passing through the grain boundary since the cyclic plastic deformation has been extended to this area.

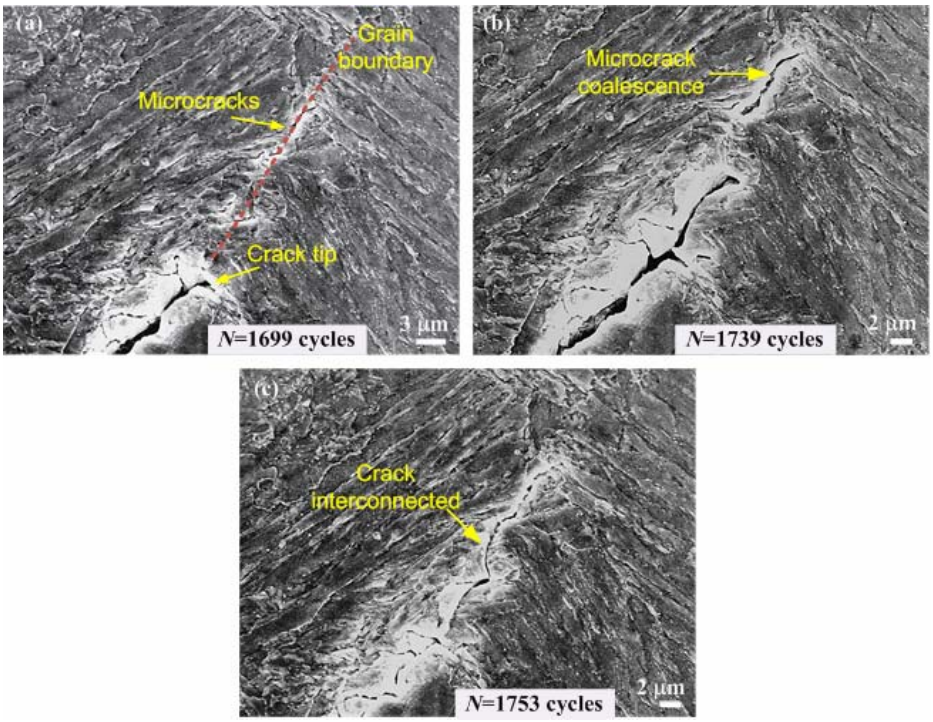

Figure 9. Coalescence of micro-cracks on the grain boundaries at the loading angle of 60°

Moreover, the damage area was dependent on the d*a*/d*N*, i.e., the higher the FCG rate, the larger the damage area. This is supported by the results in Fig. 9a, where a large number of micro-cracks has been formed at a distance about 30 μm in front of the main crack tip. Both branch and shear micro-cracks were occurred on the grain boundary. With the fatigue life increased to 1739 cycles, some micro-cracks were coalesced with each other, resulting in relatively longer cracks. Finally, all the micro-cracks were interconnected to form the main crack at N of 1753 cycles. The interconnection of grain boundary cracks increased the FCG rate considerably, which was plotted in Fig. 3. By comparing with the crack path at the loading angles of 30° and 60°, it can be observed that the length of branch cracks at α of 30° are longer and more shear micro-cracks at α of 60°. This was related to the branch versus shear crack competition in the mixed mode loading conditions.

4.2. Prediction of crack growth deflection angles

The initial deflection angles of FCG were predicted based on the SED criterion [2] in Eq. (4), the MTS criterion [1] in Eq. (5) and the criterion of Richard [4] in Eq. (6). In Eqs. (4) - (6), K_I and K_{II} are the mode I and II components, ν is Poisson's ratio, θ_0 is the critical deflection angles, and β is the angle between external loading and the crack surface. In this work, ν is set as 0.3, and the corresponding results are shown in Table 2. It is obvious that compared with the experimental data, all the predicted deflection angles for α of 30° and 60° are higher than the experimental data. Fortunately, the calculation based on MTS model was close to the experiments. Thus, the MTS criterion is suitable to predict crack growth direction in the HAZ under combined loadings. Nevertheless, all of the criteria cannot estimate the deflection of crack growth direction under pure mode I loading. This can be ascribed to the limitation of the models to homogeneous materials, and thus results in the disparities of crack deflection angle in mode I loading.

$$2(1-2\nu)\sin(\theta_0-2\beta)-2\sin\left[2(\theta_0-\beta)\right]-\sin 2\theta_0=0,\beta\neq 0 \tag{4}$$

$$K_{\mathrm{I}}\sin\theta_0+K_{\mathrm{II}}(3\cos\theta_0-1)=0 \tag{5}$$

$$\theta_0=\mathrm{m}\left[155.5°\frac{|K_{\mathrm{II}}|}{|K_{\mathrm{I}}|+|K_{\mathrm{II}}|}\right]-83.4°\left[\frac{|K_{\mathrm{II}}|}{|K_{\mathrm{I}}|+|K_{\mathrm{II}}|}\right]^2 \tag{6}$$

Table 2. Prediction of crack growth deflection angles based on different models

α	Minimum strain energy density (SED) criterion [2]	Criterion of Richard [4]	Maximum tangential stress (MTS) criterion [1]	Experiment
0	0	0	0	21°
30°	35°	28.6°	26.2°	25°
60°	55.26°	52.1°	48.98°	50°

5. Conclusions

In this study, the growth behavior of fatigue cracks in the HAZ of a welded joint under mixed mode loading conditions were studied by utilizing CTS specimens. The FCG morphology was characterized by in situ SEM observations in vacuum. The main conclusions are listed as follows.

(1) Mode I fatigue behavior in the HAZ was influenced by local microstructure anisotropy and the gradient distribution of material strength. The crack growth path tended to deflect into the lower strength weld metal, showing a “zigzag” mode.
(2) With the increasing of mixity in mode I/II fatigue loadings, FCG rate in the HAZ was decreased whereas the initial angles for crack branching were increased. Shear and branch cracks were competitive along the crack path, and fatigue crack was often initiated from grain boundary and the interface of lath martensites. Eventually the cracks tended to orient themselves into a pure mode I direction.
(3) The initial branch crack direction was predicted based on existed models, and calculation from the MTS criterion showed comparable agreement with experimental data.

Acknowledgements

The authors are grateful for the supports provided by National Natural Science Foundations of China (51205131) and the Natural Science Foundation of Shanghai (12ZR1442900). Ming-Liang Zhu would also appreciate the support from Chen Guang project (12CG33) by Shanghai Municipal Education Commission and Shanghai Education Development Foundation.

References

[1] F. Erdogan, G.C. Sih, On the Crack Extension in Plates Under Plane Loading and Transverse Shear, J Basic Eng, 85 (1963) 519-525.
[2] G.C. Sih, Mechanics of Fracture Initiation and Propagation, in, Kluwer, The Netherlands, 1991.
[3] R.J. Nuismer, An energy release rate criterion for mixed mode fracture, Int J Fract, 11 (1975) 245-250.
[4] H.A. Richard, M. Fulland, M. Sander, Theoretical crack path prediction, Fatigue Fract Eng Mater Struct, 28 (2005) 3-12.
[5] J. Qian, A. Fatemi, Mixed mode fatigue crack growth: A literature survey, Eng Fract Mech, 55 (1996) 969-990.

[6] A.K. Soh, L.C. Bian, Mixed mode fatigue crack growth criteria, Int J Fatigue, 23 (2001) 427-439.
[7] K. Tanaka, Fatigue crack propagation from a crack inclined to the cyclic tensile axis, Eng Fract Mech, 6 (1974) 493-507.
[8] Y. Xiangqiao, D. Shanyi, Z. Zehua, Mixed-mode fatigue crack growth prediction in biaxially stretched sheets, Eng Fract Mech, 43 (1992) 471-475.
[9] A.B. Patel, R.K. Pandey, Fatigue crack growth under mixed mode loading, Fatigue Fract Eng Mater Struct, 4 (1981) 65-77.
[10] D.F. Socie, C.T. Hua, D.W. Worthem, Mixed mode small crack growth, Fatigue Fract Eng Mater Struct, 10 (1987) 1-16.
[11] J.P. Campbell, R.O. Ritchie, Mixed-mode fatigue-crack growth thresholds in Ti-6Al-4V at high frequency, Scripta Mater, 41 (1999) 1067-1071.
[12] Y. Liu, S. Mahadevan, Threshold stress intensity factor and crack growth rate prediction under mixed-mode loading, Eng Fract Mech, 74 (2007) 332-345.
[13] P. Lopez-Crespo, A. Shterenlikht, J.R. Yates, E.A. Patterson, P.J. Withers, Some experimental observations on crack closure and crack-tip plasticity, Fatigue Fract Eng Mater Struct, 32 (2009) 418-429.
[14] A.M. Abdel Mageed, R.K. Pandey, Studies on cyclic crack path and the mixed-mode crack closure behaviour in Al alloy, Int J Fatigue, 14 (1992) 21-29.
[15] J.P. Campbell, R.O. Ritchie, Mixed-mode, high-cycle fatigue-crack-growth thresholds in Ti-6Al-4V: Role of bimodal and lamellar microstructures, Metall and Mat Trans A, 32 (2001) 497-503.
[16] M. Feng, F. Ding, Y. Jiang, A study of loading path influence on fatigue crack growth under combined loading, Int J Fatigue, 28 (2006) 19-27.
[17] M. Sander, H.A. Richard, Experimental and numerical investigations on the influence of the loading direction on the fatigue crack growth, Int J Fatigue, 28 (2006) 583-591.
[18] H.A. Richard, K. Benitz, A loading device for the creation of mixed mode in fracture mechanics, Int J Fract, 22 (1983) R55-R58.
[19] M.-L. Zhu, F.-Z. Xuan, Correlation between microstructure, hardness and strength in HAZ of dissimilar welds of rotor steels, Mater Sci Eng A, 527 (2010) 4035-4042.
[20] J.-K. Kim, C.-S. Kim, Fatigue crack growth behavior of rail steel under mode I and mixed mode loadings, Mater Sci Eng A, 338 (2002) 191-201.
[21] J.R. Yates, M. Zanganeh, R.A. Tomlinson, M.W. Brown, F.A.D. Garrido, Crack paths under mixed mode loading, Eng Fract Mech, 75 (2008) 319-330.
[22] J. Tong, J.R. Yates, M.W. Brown, The formation and propagation of mode I branch cracks in mixed mode fatigue failure, Eng Fract Mech, 56 (1997) 213-231.